Nanoparticle Stability in Polymer Melts As Determined by Particle Second Virial Measurement

Benjamin J. Anderson and Charles F. Zukoski*

Department of Chemical and Biomolecular Engineering, University of Illinois at Urbana−Champaign, 600 South Mathews Ave, Urbana, Illinois 61801

Received October 21, 2006; Revised Manuscript Received May 15, 2007

ABSTRACT: The stability of 44 nm diameter silica particles in poly(ethylene glycol) (PEG) melts is assessed through the experimental measurement of particle second virial coefficients, $B_2 = B_{2,cc}/B_2^{HS}$, where $B_{2,cc}$ is the particle second virial coefficient and B_2^{HS} is the excluded volume second virial coefficient of the particles. Measurements are made using side bounce ultra-small-angle X-ray scattering (SBUSAXS) of dilute filled PEG melts of variable molecular weight. Results show B_2 values to be equal to or greater than one for the molecular weights investigated. Experimental results are compared to recent PRISM theory adaptations to filled polymer melts.

I. Introduction

Filled polymers are a class of materials in which particulate matter is dispersed in a polymer matrix. These materials are of significant technological interest due to the ability of the particles to improve and alter mechanical, electrical, rheological, optical, and/or thermal properties of the composite. These materials find uses in diverse products, including filled rubbers, nanocomposites, insulating and conductive polymers, biomaterials, coatings, and thermal resistive materials. Many of the particle enhanced properties are strongly dependent on the state of the particle dispersion. In turn, the degree of dispersion is determined by polymer-mediated particle interactions. Only a few studies have investigated the microstructure of these systems.[1−5]

Comparison between models and experimental measures of particle behavior in polymer melts is made difficult due to the long relaxation times associated with high molecular weight polymers and difficulties in reaching equilibrium. To circumvent this difficulty, we work with nanoparticle dispersions in low molecular weight polymers where we systematically increase polymer molecular weight. Using side bounce ultra-small-angle X-ray scattering experiments (SBUSAXS),[6] we assess the thermodynamic stability of 44 nm diameter Stöber silica particles in poly(ethylene glycol) (PEG) melts through the determination of second virial coefficients. Our dilute polymer melt studies lay the foundation for future studies of the microstructure of dense particulate−polymer mixtures.

PEG is a highly active surface molecule able to adsorb strongly to hydrophilic and hydrophobic surfaces often irreversibly.[7−21] PEG adsorption capability has been an area of active research from fundamental studies on polymer adsorption and colloid stability[8−10,12−18,21] to novel innovative areas such as drug delivery and adsorption inhibition.[11,19] In the area of biotechnology and drug delivery, proteins are conjugated with PEG to increase their transfer to a surface.[11] In other cases, PEG adsorption may be used to inhibit adsorption of another molecule.[19] A few studies have also shown that end effects alter the adsorption characteristics of the PEG backbone even at high molecular weights.[22−24] Measurement of segmental adsorption energies and estimates of the work of adhesion of PEG on silica show PEG to adsorb strongly to a silica surface, much more so than other polymers.[20] These studies tend to be carried out in ternary systems containing solvent, particles, and polymer. We are interested here in understanding polymer-mediated particle interactions in a binary system of particles and polymer.

Recently, a model for the state of aggregation of nanoparticles in polymer melts has been developed by Hooper and Schweizer.[25] This model uses a polymer reference interaction site model (PRISM) for the polymer and accounts for polymer segment−segment, polymer segment−particle, and particle−particle interactions. For particles that only experience volume exclusion interactions, two key parameters are found to be important in determining the state of particle aggregation: the polymer segment−particle contact interaction energy and the range of the attraction. The state of aggregation is determined by a competition between entropic and enthalpic contributions where the entropic contribution results from oscillatory depletion forces acting between two particles in a polymer melt. Depletion forces are governed by intrinsic polymer density fluctuations that arise as a result of segment level packing correlations. Depletion forces will therefore depend on the ratio of particle to segment diameters, D/d. These attractive forces favor contact aggregation and describe the athermal limit where there is negligible interaction between polymer segment and the particle surface. This type of behavior is similar to the strong depletion forces found in highly asymmetric binary hard-sphere suspensions[26,27] and in nonadsorbing dilute polymer−particle solutions[28−32] where contact aggregation of the large spheres is driven by exclusion of the small spheres or polymer from the region between the large spheres. The structure and potential of mean force between two particles in the athermal case have recently been explored using PRISM theory and molecular dynamic simulations.[33] Good agreement was seen between the two approaches.

The enthalpic contribution becomes important when there is a favorable attraction between monomer and the particle surface. For particles experiencing only volume exclusion interactions, a favorable polymer−particle attraction competes against entropic depletion and, as has long be appreciated, is necessary for obtaining a stable dispersion in a polymer melt.[34] As the strength and range of the polymer−particle attraction are

* Corresponding author. E-mail address: czukoski@uiuc.edu.

10.1021/ma0624346 CCC: $37.00
Published on Web 06/15/2007

increased, one can imagine the buildup of an immobilized polymer layer that resists direct particle contact and results in steric stabilization.

Recent studies performed by Hooper and Schweizer suggest four types of particle organization in dilute particle−polymer melts: entropic depletion aggregation, steric stabilization, local bridging flocculation, and tele-bridging flocculation.[25] The ability of a given polymer−particle mixture to fall into one of these classes is governed by the particle−polymer segment size ratio, particle volume fraction ϕ_c, polymer molecular weight, and the strength ϵ_{pc} and range α of attraction between polymer segments and the particle surface. Hooper and Schweizer also investigate particle stability in polymer melts through calculation of the particle second virial coefficient.[35] They find the second virial coefficient displays nonmonotonic behavior varying from negative to positive and back to negative with increases in the strength of polymer−particle attraction for specified polymer chain length N. The repulsive regime corresponding to positive second virial coefficients occurs at interaction energies of 1−2 k_BT between polymer segments and the particle surface. Note that this interaction energy is referenced to the polymer segment−segment interactions in the bulk. The transition from attractive to repulsive (negative to positive second virial coefficient) is abrupt at low polymer−particle attraction (<0.5 k_BT) while the transition from repulsive to attractive (positive to negative second virial coefficient) depends on additional mixture parameters such as D/d, α, and N. Few studies are available to test the predictions of this model.

Below we characterize the second virial coefficient of silica nanoparticles as a function of polymer molecular weight in the melt. We start with monomer and increase the degree of polymerization, N, to 180. These studies are carried out in the high D/d limit and under conditions where we expect the strength of polymer segment−particle interactions to be attractive.

This paper is structured as follows. Experimental methods are described in section II. In section III, we report the details of extracting the second virial coefficient and its variation with polymer molecular weight. We find that the normalized particle second virial coefficient $\bar{B}_2$ ($\bar{B}_2 = B_{2,cc}/B_2^{HS}$ where B_2^{HS} is the hard-sphere value) is greater than or approximately equal to one for all molecular weights sampled. This indicates that the nanoparticles are more repulsive than their equivalent hard-sphere value. Thus, the nanoparticles appear to be thermodynamically stable in a PEG melt irrespective of molecular weight. In section IV, we discuss the experimental results in relation to PRISM theory. Conclusions are drawn in section V.

II. Experimental Methods

A. Sample Preparation. Silica particles were synthesized by the base-catalyzed hydrolysis and condensation of tetraethylorthosilicate according to the method of Stöber et al.[36] The synthesis produces an alcosol solution of silica particles. Particle diameter was 43 ± 4 nm determined from TEM measurements (number distribution) and 44 ± 4 nm determined from X-ray scattering measurements (volume distribution). We predict a particle to segment size ratio of 60 on the basis of a Kuhn segment diameter of 0.7 nm ($d = C_\infty l/\cos(\theta_p/2)$, where $C_\infty = 4.1$ is the characteristic ratio of PEG, $l = 1.5$ Å is the length of a backbone bond, and $\theta_p = 68°$ is the angle of a backbone bond). Large D/d values are equated with decreased particle stability. A particle diameter of 44 nm was chosen as a compromise between minimizing D/d and our ability to synthesize well-defined monodisperse particles. Particles were dispersed in ethylene glycol and PEG ranging in MW from 400 to 8000 purchased from Sigma-Aldrich. Particle dispersions were made by combining known masses of the alcosol and PEG. The ethanol is evaporated at ~70 °C in a vacuum oven initially purged with nitrogen to remove oxygen which is known to degrade the polymer at elevated temperature. Higher temperatures are needed for PEG to dissolve in ethanol. The unusual phase behavior of PEG in ethanol has recently been studied.[37]

The amount of alcosol added to a known mass of PEG was determined by the desired amount of loading once the ethanol was evaporated. The filled polymer is transparent since PEG and silica are contrast matched. This index matching reduces the van der Waals forces between the particles.[38] The filler content of the alcosol was measured by dry weights after evaporation of the ethanol. The volume fractions of filler were determined from the mass of silica added to the polymer adopting a particle density of 1.6 g/cm^3. The particle density was determined from light scattering of silica nanoparticle dispersions in ethylene glycol.

B. Light Scattering. Static light scattering (SLS) was performed on a Brookhaven Instruments BI-200 SM goniometer with a Lexel Argon-Ion model 95 laser. The wavelength λ was 514 nm, and measurements were taken from $\theta = 50°-130°$. The instrument was calibrated with the scattering of toluene to convert scattering intensity from counts per second to absolute units of cm^{-1}. The samples were filtered with 0.45 μm Corning filters into glass tubes with a beam path length of 1 cm. The samples were heated to 70 °C and maintained by a constant temperature bath. Light intensity was measured by a photomultiplier tube and processed by a BI-9000AT digital correlator. SLS was performed on very dilute particle concentrations (2.4, 4.8, 9.0, 11.9, and 14.1 mg/mL) in ethylene glycol (EG). SLS of the filled polymer was not practical due to the difficulty of filtering polymer to remove dust. PEG and silica are also nearly contrast matched which further complicates the measurement. The refractive index of EG is slightly less than that of silica, making it possible to see the particles with light.

C. SBUSAXS. SBUSAXS was performed at the 33ID-D beamline UNI-CAT facility located at the Advance Photon Source, Argonne National Laboratory. The instrument employs a Bonse-Hart camera and a double-crystal Si(111) optics to extend the range of measurements to lower scattering vectors. The side bounce characteristic is enabled by a pair of horizontally reflecting crystals which enabled effective pinhole collimation removing the need for slit desmearing. An absolute calibration converts scattering intensity from counts per second to absolute units of cm^{-1} through knowledge of the sample thickness along the path of the beam. Samples were loaded in custom-made aluminum cells. Two Kapton polyimide slides sealed the sides of the cell chamber. The incident beam passes through the first Kapton slide, is scattered by the sample, and exits through the second Kapton slide. The beam path length was ~1 mm. The cells were heated to 70 °C, which is above the melting temperature of PEG (66 °C), and maintained by a constant temperature bath. Measurements on each sample were taken over a period of 30 min. Background intensity was accounted for by measuring the scattered intensity of neat PEG. The scattering intensity of the PEG is subtracted off of the sample scattering, leaving only scattering due to the silica nanoparticles. This is based on the fact that the scattering from the silica particles dominates, leading to our assumption that the dispersion can be viewed as an effective one-component system.

III. Results

A. Light Scattering. Static light scattering was performed on silica dispersions in EG as a check of the particle molecular weight that can be used to calculate the particle density. The scattering intensity of light from a single-component dispersion written in terms of particle mass concentration is given by

$$R(q,c) = cMKP(q)\,S(q,c) + B \tag{1}$$

$R(q,c)$ is the Rayleigh ratio which is the scattered intensity normalized by the incident intensity. The Rayleigh ratio was determined by normalizing the scattering intensity to that of

pure toluene at 90°. The variable q is the scattering vector, $q = (4\pi/\lambda)\sin(\theta/2)$ where λ is the incident beam wavelength and θ is the scattering angle. The first term refers to scattering from the particles where c is the particle mass concentration, M is the particle molecular weight, and K is an optical constant, $K = 2\pi^2 n^2 (dn/dc)^2/N_A\lambda^4$, where n is the refractive index of EG, dn/dc is the refractive index increment, and N_A is Avrograd o's number. The value of dn/dc of silica in ethylene glycol was measured with a Milton Roy refractomenter to be 0.0219 cm^3/g. $P(q)$ is the form factor accounting for intraparticle scattering interference, and $S(q,c)$ is the structure factor accounting for interparticle scattering interference. The second term, B, refers to background scattering of the dispersing phase. Background scattering is subtracted off of the Rayleigh ratio by the scattering of pure EG. From this point on, $R(q,c)$ will refer only to scattering from the particles.

To measure the particle molecular weight, we are interested in scattering in the zero angle and zero concentration limit. We assume the particle form factor is well described by Guinier's law ($qD_z < 2$):

$$P_z(q) = 1 - \frac{5}{9}\left(\frac{qD_z}{2}\right)^2 + O(q^4 D_z{}^4) \qquad (2)$$

where D_z is the z-average particle diameter. Under conditions of small q, a suitable approximation drops higher order terms which scale as q^4 and higher. In addition, in the $q \to 0$ limit, the structure factor can be related to a virial expansion through the osmotic compressibility

$$\lim_{q\to 0}\frac{1}{S(q,c)} = \frac{M}{N_A k_B T}\frac{\partial \Pi}{\partial c} = 1 + \frac{2B_{2,cc}N_A}{M}c + \frac{3B_{3,cc}N_A{}^2}{M^2}c^2 + \ldots \qquad (3)$$

In the dilute limit, higher order terms may be dropped.

$$\lim_{q\to 0}\frac{1}{S(q,c)} = \frac{M}{N_A k_B T}\frac{\partial \Pi}{\partial c} = 1 + \frac{8\bar{B}_2 N_A V_c}{M}c \qquad (4)$$

Here $\bar{B}_2 = B_{2,cc}/B_2^{HS}$ where the second virial coefficient is divided by that of a hard sphere of the same size. The hard-sphere value is equal to 4 times the particle volume, $B_2^{HS} = 4V_c$. Substituting these two approximations into eq 1, we rewrite the Rayleigh ratio in Zimm form[39]

$$\frac{cK}{R(q,c)} = \left[1 + \frac{5}{9}\left(\frac{qD_z}{2}\right)^2\right]\left[\frac{1}{M_w} + \frac{8\bar{B}_2 N_A V_c}{M_w{}^2}c\right] \qquad (5)$$

In accordance with eq 5, the data are plotted with $cK/R(q,c)$ as the ordinate and $q^2 + c$ as the abscissa. By applying the limits of $q = 0$ and $c = 0$, the data can be extrapolated to obtain estimates of $cK/R(q,c)$ at a single concentration and single scattering vector, respectively (see Figure 1). The $q = 0$ extrapolated points have a slope that depends on B_2 and an intercept of $M_w{}^{-1}$. We find $\bar{B}_2 = 10.3 \pm 0.5$ and $M_w = (4.5 \pm 0.2) \times 10^7$ g/mol. A $\bar{B}_2$ of 10.3 corresponds to an effective hard-sphere diameter of 96 nm. The $c = 0$ extrapolated points have a slope that depends on D_z and an intercept of $M_w{}^{-1}$. We find a D_z of 45 ± 5 nm and a $M_w = (4.5 \pm 0.1) \times 10^7$ g/mol. The weight-average molecular weights are the same in both limits. The weight-average molecular weight divided by the z-average particle size gives a silica density of 1.6 g/cm^3 as anticipated from the literature.[40]

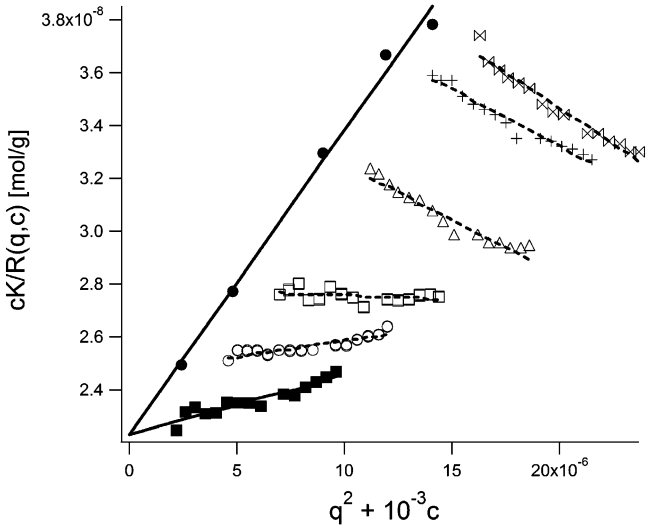

Figure 1. Zimm plot of silica in EG at concentrations c of 2.4 (○), 4.8 (□), 9.0 (△), 11.9 (+), and 14.1 mg/mL (⋈) with a stretch factor of 10^{-3}. The closed symbols show the extrapolated values for zero angle (●) and zero concentration (■). The lines show the fits to the extrapolated data for zero angle (solid) and zero concentration (dotted).

The reader may be concerned about the three higher concentration data sets having a negative slope. This negative slope is due to interparticle structure having an effect on scattering and appears in the structure factor as a square angular dependence.[41−44]

$$\frac{1}{S_z(q,c)} = \frac{1}{S(0,c)} - \gamma(c)(qD_z)^2 + O(qD_z)^4 \qquad (6)$$

For the case of repulsive spheres, $\gamma(c)$ is always a positive function of concentration.[44] The second virial coefficient suggests that the particles appear more than twice as large with respect to diameter than their real size. This will cause particle structure to build into the suspension at concentrations lower than what would be expected for purely hard-sphere systems. Without accounting for the angular dependence of the structure factor, the negative slopes seen at high concentration might be thought to imply a negative $D_z{}^2$. The slopes are instead a result of the square angular dependence of the structure factor. The angular dependence of the structure factor drops out in the zero angle and zero concentration limits, allowing us to obtain the second virial coefficient and a particle size consistent with TEM measurements.

Before presenting the second virial results of silica particles in PEG melts, we turn first to explaining the large $\bar{B}_2$ value in EG. The $\bar{B}_2$ is significantly larger than unity, which tells us that the particles appear much bigger than their actual size. We hypothesize that the dielectric constant of EG is sufficiently high that the particles can carry a charge. To test the hypothesis, the conductivity of dilute particle suspensions in EG and PEG400 was measured as a function of particle volume fraction. Conductivity measurements were made using a YSI model 34 conductance−resistance meter with a model 3403 dip cell at 25 °C. In the dilute particle limit where particles are noninteracting, we approximate the suspension conductivity as arising from all ionic species according to

$$\sigma = \sigma_s + \sum_{k=1}^{4} z_k e \omega_k \rho_k \qquad (7)$$

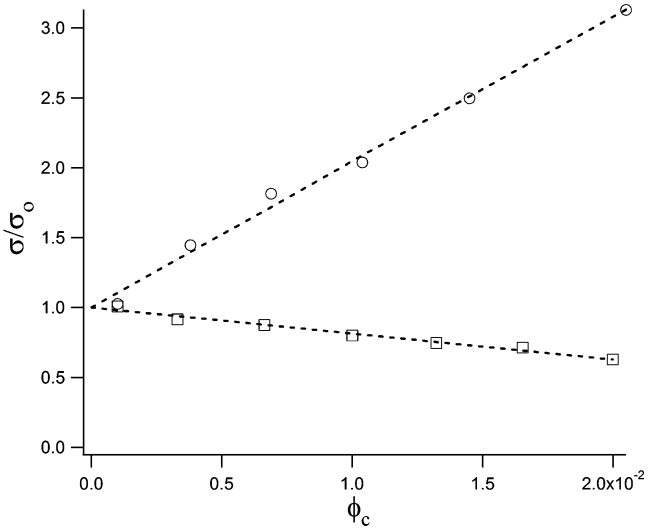

Figure 2. Reduced conductivity as a function of particle volume fraction for EG (○) and PEG400 (□). Dashed lines show a linear fit.

In this equation, σ is the solution conductivity, σ_s is the conductivity of pure EG, z_k and ω_k are the valence charge and mobilities of the kth ion, ρ_k is the bulk number concentration of the kth ion, and e is the elementary charge of an electron. Ion mobility is defined by the relation

$$\omega_k = \frac{z_k e}{6\pi\mu a_k} \tag{8}$$

Here z_k and a_k are the valence and radius of the kth ion, respectively, and μ is the continuous phase viscosity. There are four general ionic species that contribute to the solution conductivity: positive and negative ions present other than those contributed by the particles, particle counterions due to dissociation of silanol groups at the particle surface ($SiOH \rightarrow SiO^- + H^+$), and the particle macroion. More complex expressions for solution conductivity as a function of particle concentration exist, but this simple expression will serve our purpose.

The conductivity of pure EG is grouped with the first two terms of the summation in eq 7 to give the conductivity of the solution at infinite particle dilution, σ_0. The EG suspensions contain trace amount of ammonia that was present in the alcosol solution before the ethanol is evaporated off. Also, because of the need to maintain overall solution neutrality, particle counterions, i, must balance particle charge, $\rho_i = z_c\rho_c$. We apply these substitutions to eq 7 and rewrite in terms of particle volume fraction, ϕ_c.

$$\sigma = \sigma_0 + \frac{z_c z_i e\omega_i + z_c e\omega_c}{(\pi/6)D_s^3}\phi_c \tag{9}$$

D_s is the diameter of the particle at the Stern surface. Ion mobility is estimated in EG by multiplying a standard mobility of an ion in aqueous (K^+/Cl^- ion, $\omega_{i,aq} = 7.8 \times 10^{-4}$ cm^2/(V s)) by the ratio of the continuous phase viscosities

$$\omega_{i,EG} = \omega_{i,aq}\frac{\mu_{aq}}{\mu_{EG}} \tag{10}$$

We assume the valence charge of an ion to be one. Particle charge can be determined from the slope of conductivity measured as a function of particle volume fraction with knowledge of the particle mobility. Particle mobilities are commonly measured using electrophoresis techniques. These techniques require high contrast between the particles and dispersing phase. We were unable to measure the electrophoretic mobility of our particles in EG due to the small particle size and similar refractive indices between silica and EG. Therefore, we use the Hückel equation

$$\omega_c = \frac{2}{3}\frac{\epsilon_r\epsilon_0\varsigma}{\mu} \tag{11}$$

to estimate the particle mobility in EG. ς is the zeta potential which is defined as the potential at the surface of shear near the particle surface.

If we assume a thick double layer, $\kappa D_s/2 \ll 1$, the zeta potential can be assumed to be analogous with the particle surface potential. The particle surface potential is related to particle charge through the solution to the linearized Poisson−Boltzmann equation[45]

$$\varsigma = \frac{z_c e}{2\pi\epsilon_r\epsilon_0 D_s}\exp[-\kappa D_s/2] \tag{12}$$

where κ is the Debye parameter

$$\kappa = \left(\frac{e^2}{\epsilon_r\epsilon_0 k_B T}\sum_k z_k^2\rho_k\right)^{1/2} \tag{13}$$

Assuming a monovalent symmetrical electrolyte, ρ_k was estimated from σ_0 to be of the order 10^{-4} M, giving a $\kappa D_s/2 \approx 1$. Substituting eqs 11 and 12 into eq 9 gives a linear equation for the conductivity as a function of particle volume fraction with a slope that depends on the zeta potential:

$$\sigma = \sigma_0 + \frac{12\epsilon_r\epsilon_0}{D_s^2\exp[-\kappa D_s/2]}\left[z_i\omega_i\varsigma + \frac{2\epsilon_r\epsilon_0}{3\mu}\varsigma^2\right]\phi_c \tag{14}$$

In Figure 2, the reduced conductivity is plotted as a function of particle volume fraction. We find the conductivity to rise with the addition of particles to EG, indicating that the particles add charge to the suspension. Using eq 14, we estimate a zeta potential of 100 mV, which according to eq 12 translates into 400 elementary charges per particle. We find the opposite to be true in PEG400. The conductivity declines with the addition of particles, indicating that the dispersing phase conducts more so than the particles. This shows that the surface silanol groups do not disassociate in PEG and the particles are not charged. The decline, however, is much steeper than we would expect for simply uncharged particles, leaving us to believe that some additional mechanism is also contributing to the reduction in conductivity of the filled polymer. The conclusion we draw is that ethylene glycol has a large enough permittivity, $\epsilon_{EG} = 38.7$, to support a small charge on the particle surface while PEG400 where $\epsilon_{PEG} \approx 5-8$ cannot support appreciable charge.

As a check on this estimate of particle surface potential, we use the zeta potential to calculate $\bar{B}_2$ and directly compare the value with the results of light scattering. The $\bar{B}_2$ of a charged particle is related to the repulsive potential force, $\Phi(r)$, between two interacting double layers[38]

$$\bar{B}_2 = \frac{1}{D_s^3}[D_s + \int_{D_s}^{b}(1 - \exp[\Phi(r)/k_B T])\,dr]^3 \tag{15}$$

The integration variable b is the outer limit where the repulsive potential decays to zero. The repulsive potential force between two interacting double layers is approximated as

$$\frac{\Phi(r)}{k_B T} = \delta \frac{\exp[-\kappa r]}{\kappa r} \tag{16}$$

with $\delta = \pi\epsilon_r\epsilon_0\varsigma^2 D_s^2 \kappa \exp[\kappa D_s]/k_B T$.[38] Evaluating the integral with $\varsigma = 105$ mV and $\kappa D_s/2 = 1.9$ gives $\bar{B}_2 \sim 10$, which supports the second virial measured with light scattering. These results provide independent and consistent support for particle charge in EG.

It is widely known that the molecular weight of colloidal macroions determined by light scattering can be heavily influenced by double layer overlap of adjacent particles.[46] Double layer overlap will cause a disorder−order transition at volume fractions much lower than expected for hard spheres where the crystallization volume fraction is 0.5. Strong double layer overlap leads to correlated fluctuations in particle density.[38] Under these circumstances, density fluctuations giving rise to the scattering are not independent such that eq 5 cannot be applied. Two approaches can be used to avoid this difficulty. First, the repulsions can be screened by increasing the background electrolyte concentration. The amount of electrolyte required to screen the electrostatic repulsions will depend on particle charge. The higher the charge, the larger the concentration of background electrolyte required to mitigate the effects of self-screening. Swamping with excess electrolyte, however, may cause scattering from the electrolyte to become significant compared to the particle. Scattering from excess electrolyte can be taken into account by adding an additional term to eq 1[47]

$$R(q,c) = \frac{cK}{M}\left[M - \frac{z_c e \sum c_j z_j e_j}{\sum (c_j/M_j) z_j^2 e_j^2}\right]^2 P(q)\, S(q,c) + B \tag{17}$$

The subscript j refers to the added excess electrolyte. At low ionic strengths, the added term in eq 17 is negligible as in our case. In the second approach, double layer overlap can simply be avoided by reducing the macroion concentration such that eq 5 is valid to determine molecular weight and the second virial coefficient.[46,47] For charged particles, the capacity of the solution to screen double layer repulsions is a function of the particle concentration. At sufficiently low concentrations, density fluctuations in the charged particles will become uncorrelated. The challenge is to determine the volume fraction range where the particle density fluctuations become independent such that accurate extrapolation to zero concentration can be made. Experimentally, one can look for linearity in $1/S(0,c)$ vs c, which is observed (Figure 1). In addition, we can estimate whether significant double layer overlap should be expected. This is done by calculating the volume fraction where the particles will undergo a disorder-to-order transition. Hard-sphere suspensions transition from a disordered state at $\phi_c > 0.50$ to an ordered state at $\phi_c > 0.55$. The larger effective size of our particles will cause this transition to occur at a lower ϕ_c given by the expression $0.50\bar{B}_2 < \phi_c < 0.55\bar{B}_2$. Thus, we can expect double layer overlap to be a concern at $\phi_c \approx 0.05$. The volume fractions probed by light scattering are all less than 1%. Thus, the effects of double layer overlap resulting in nonlinearities are not expected and, as shown, not observed. The linearity of the $1/S(0,c)$ extrapolated points at different concentrations shown in Figure 1, and this estimate of the particle concentration where significant double layer overlap will occur indicates that at silica volume fractions less than 0.01 in ethylene glycol we are in a limit where density fluctuations are sufficiently uncorrelated that we can extrapolate to zero concentration to determine an accurate molecular weight. The agreement of this molecular weight with other literature values of particle density suggests that we have a consistent estimate of particle molecular weight to be used in X-ray scattering experiments.

B. SBUSAXS. The scattering intensity of X-rays from a single-component dispersion is similar in form to that used for light written in terms of particle volume fraction

$$I(q,\phi_c) = \phi_c V_c \Delta\rho_e^2 P(q)\, S(q,\phi_c) + B \tag{18}$$

The first term refers to scattering from the particles where V_c is the volume of a single particle and $\Delta\rho_e$ is the electron scattering length density of the particles over that of the PEG dispersing phase. Again, the variable q is the scattering vector, $P(q)$ is the form factor, and $S(q,\phi_c)$ is the structure factor. Background scattering is subtracted off of the intensity by the scattering of the neat polymer. From this point on, $I(q,\phi_c)$ will refer only to scattering from the particles.

Because of its larger scattering length density, silica scatters much more strongly than the polymer with configurations altered by the particles. As a result, scattering from conformational changes in the polymer matrix caused by the particles is negligible in the experimental measure of the particle second virial coefficient. This approach is equivalent to scattering studies of suspensions in low molecular weight continuous phases where distortions to the solvent packing due to the presence of the particles are associated with the particle and ultimately attributed to particle size or potential of mean force.[48−51] Hooper and Schweizer show that ignoring the effects of polymer configurational changes in calculating $B_{2,cc}$ results in only moderate shifts in theoretical predictions of filled polymer melt phase behavior.[35]

In the dilute particle limit, the structure factor goes to unity and the scattering equation reduces to $I(q,\phi_c) = \phi_c V_c \Delta\rho_e^2 P(q)$. The full form factor for spherical particles is given by

$$P(q) = \left(3\frac{\sin(qD/2) - (qD/2)\cos(qD/2)}{(qD/2)^3}\right)^2 \tag{19}$$

We account for modest polydispersity by calculating $P(q)$ for a volume distribution in particle size. This is done here by employing a Gaussian diameter distribution to calculate an average form factor for a population of particles with mean diameter $\bar{D}_v$ and standard deviation σ_v. The subscript v indicates volume distribution. The integration variable D_v is the variable diameter of a particle.

$$\bar{P}_v(q) = \frac{\int \frac{1}{\sqrt{2\pi\sigma^2}} e^{-(D_v-\bar{D}_v)^2/2\sigma^2} D_v^6 P(q)\, dD_v}{\int \frac{1}{\sqrt{2\pi\sigma^2}} e^{-(D_v-\bar{D}_v)^2/2\sigma^2} D_v^6\, dD_v} \tag{20}$$

Experimental scattering of dilute suspensions is fit to eq 18 by minimizing the sum of the residuals and utilizing eq 20 for the form factor to determine a scattering size and standard deviation in the polymer melt (Figure 3). The fitting procedure has three adjustable parameters: particle diameter, standard deviation, and electron contrast density. The fitting routine yielded a particle diameter of 44 nm and a standard deviation of 4 nm for all polymer molecular weights. The electron contrast, however, is not the true contrast but is merely a variable parameter used in fitting the data with an average form factor. $S(q,\phi_c)$ is not truly unity and only approaches unity in the limit $\phi_c \rightarrow 0$. Still, the influence of $S(q,\phi_c)$ on scattering is small

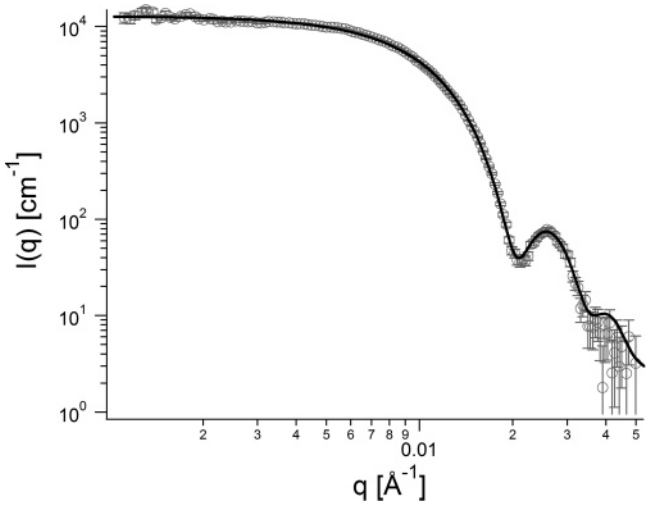

Figure 3. Experimental scattered intensity (○) and model fit (solid line) of a dilute suspension ($\phi_c = 0.05$) of particles in PEG3000. Mean particle diameter $\bar{D}_v$ and size distribution σ are extracted from the model fit utilizing an average form factor $\bar{P}_v(q)$.

enough compared to $P(q)$ that we are able to fit the data and get a size and standard deviation that are comparable with TEM measurements.

To extract second virial coefficients from the scattering results, we are interested in variations in absolute scattering intensity in the zero angle limit. To determine this, we need to know the particle volume V_c, the particle volume fraction ϕ_c, and the electron contrast density $\Delta\rho_e$. The particle volume can be derived from the form factor fit (see Figure 1) and also calculated from TEM measurement. Particle volume fraction is calculated from the mass of particles added to the polymer and the particle molecular weight (determined with light scattering). We lack an independent measure of the electron contrast density and must determine it simultaneously with the second virial coefficient. (The analogous parameter with light is dn/dc, which is measured using a refractometer.) The scattering intensity is written in a form similar to eq 5 after substituting eqs 2 and 4 into eq 18

$$\frac{\phi_c V_c}{I(q,\phi_c)} = \left[1 + \frac{5}{9}\left(\frac{qD_z}{2}\right)^2\right]\left[\frac{1}{\Delta\rho_e{}^2} + \frac{8\bar{B}_2}{\Delta\rho_e{}^2}\phi_c\right] \qquad (21)$$

In Figure 4, scattering intensity is plotted vs qD_z for filled PEG3000. $I(q,\phi_c)$ data in the qD_z range of 0.7−2.0 is fit to eq 21. Applying the limits of $q = 0$ and $\phi_c = 0$, we calculate $\phi_c V_c / I(q,\phi_c)$ at a single particle volume fraction and single scattering vector, respectively. Figure 5 shows data for PEG3000 plotted according to eq 21. The $q = 0$ extrapolated points have a slope that depends on $\bar{B}_2$ and an intercept of $\Delta\rho_e{}^{-2}$. We find $\bar{B}_2 = 1.5 \pm 0.8$ and $\Delta\rho_e = (8.4 \pm 0.8) \times 10^{10}$ cm^{-2}. The $c = 0$ extrapolated points have a slope that depends on D_z and an intercept of $\Delta\rho_e{}^{-2}$. We find a D_z of 44 ± 12 nm and a $\Delta\rho_e = (8.4 \pm 0.3) \times 10^{10}$ cm^{-2}.

A consistency check on the data is that we expect $\Delta\rho_e$ to be the same for all molecular weights of PEG. The electron contrast between molecular silica and PEG as calculated from the atomic electron density is 8.23×10^{10} cm^{-2}. As seen in Table 1, our expectation for a constant electron density as MW is varied is met, and the experimental and calculated values are the same within experimental uncertainty. In addition, Table 1 contains second virial coefficients for the particles in monomer (EG) and in polymer of increasing MW. We find the particles in polymer interact with excluded volumes greater than or approximately

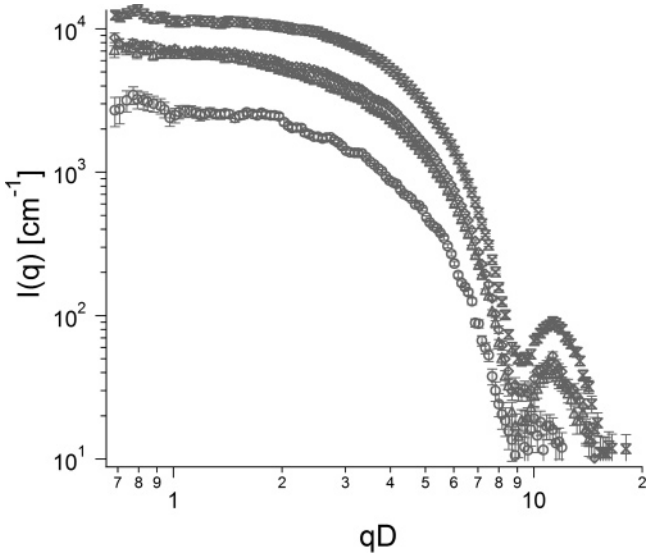

Figure 4. Experimental scattering intensity for particle volume fractions ϕ_c of 0.01 (○), 0.03 (△), 0.04 (◇), and 0.05 (⋈) in PEG3000.

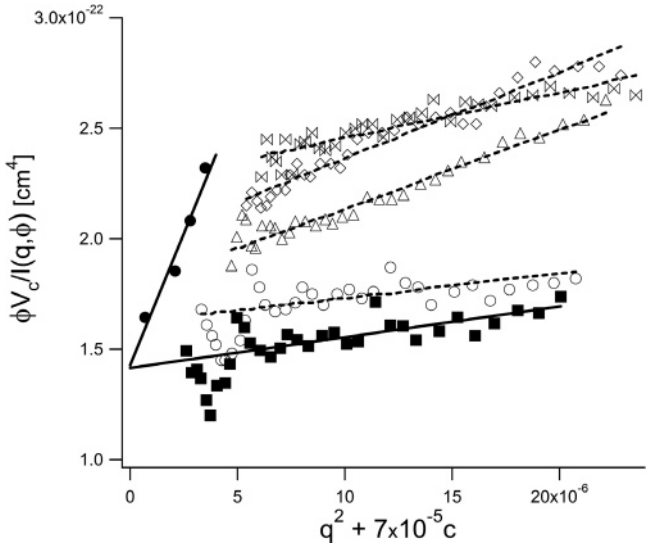

Figure 5. Zimm plot of silica in PEG3000 with ϕ_c of 0.01 (○), 0.03 (△), 0.04 (◇), and 0.05 (⋈) and a stretch factor of 7×10^{-5}. The closed symbols show the extrapolated values for zero q (●) and zero ϕ_c (■). The solid lines show fits to the extrapolated data for zero q and zero ϕ_c. Dotted lines show linear fits to the experimental data at each ϕ_c.

equal to the hard-sphere value. Our methods of extracting the second virial coefficient of the particles in ethylene glycol using SBUSAXS were unsuccessful due to a large degree of suspension structure being observed even at volume fractions of a few percent due to surface charge. (Indeed, particle structure was even observed with light at volume fractions of less than 1%.). As a result, very dilute concentrations were needed to study suspensions under conditions where only pair interactions are important. At these concentrations, the X-ray scattering from particles is too weak to obtain accurate data. Therefore, the table presents the second virial coefficient measured with light scattering to compare with PEG.

IV. Discussion

As shown in Table 1, for all N greater than 1, the second virial coefficient is equal to or slightly greater than unity. The values of $\bar{B}_2$ and the angular dependence of the scattering from the melts show no evidence of aggregation. The absence of

Table 1. Second Virial Coefficient and Electron Contrast Measurements

MW	EG[a]	400	1000	2000	3000	4000	6000	8000
N	1	9	23	45	68	91	136	182
$\bar{B}_2$	10.3 ± 0.5	1.2 ± 0.7	1.5 ± 0.5	1.3 ± 0.8	1.5 ± 0.8	1.3 ± 0.5	1.5 ± 0.8	1.0 ± 0.8
$\Delta\rho_e$ [$\times 10^{10}$ cm^{-2}]		8.5 ± 0.9	7.6 ± 0.8	8.1 ± 1.2	8.4 ± 0.8	8.3 ± 1.5	9.0 ± 0.7	8.2 ± 0.9

[a] Determined with light scattering.

attractions can be partially attributed to the index matching of the particles and polymer which greatly reduces the van der Waals contribution to attractions.[38] From the calculations of Hooper and Schweizer, we would expect strong depletion attractions if the polymer and particles interact in the athermal limit. Thus, even in the absence of van der Waals attractions, we would expect strong attractions. We also know that PEG adsorbs strongly to silica from solution,[12−14,17] indicating that the particle stability may arise from steric stabilization.

In this event, Hooper and Schweizer from PRISM calculations suggest that for a range of polymer segment−particle attractive strengths the potentials of mean force between the particles are oscillatory with periods on the order of the segment diameter, d. Integrating over these to determine the effective excluded volume has a net result of yielding second virial coefficients close to unity independent of D/d and N.[25] While it is deceptively easy to assume that $\bar{B}_2 = 1$ indicates that the particles interact with only volume exclusion interactions, the work of Hooper and Schweizer suggests that this is a fortuitous summation over the positive and negative oscillating contributions to the potential of mean force (PMF) that results in $\bar{B}_2$ values close to unity.[35]

Hooper and Schweizer predict conditions resulting in repulsive particles (i.e., $\bar{B}_2 > 0$) are bordered by unstable regions where $\bar{B}_2$ values plummet to extreme negative values. Effective hard-sphere $\bar{B}_2$ values occur at modest ϵ_{pc}, strong enough to prevent particle contact aggregation but weak enough to resist polymer-mediated network formation. Phase diagrams worked out by Hooper and Schweizer summarize the values of $\bar{B}_2$ resulting in a miscibility window where filler particles are stabilized by steric repulsions of adsorbed polymer layers (see Figures 6 and 7 in Hooper and Schweizer[35]). This window occurs at modest polymer−particle surface interaction and is bordered by direct contact aggregation from weak interaction and particle−particle bridging caused by strong interaction. The spinodial boundaries that determine the width of the miscibility window are sensitive to variables D/d and N. Increasing either variable leads to a narrowing of the miscibility window. The narrowing of the miscibility window with increasing D/d appears to be more significant than for increasing N. A direct comparison of our experimental system to the PRISM model would predict silica-filled PEG to fall in the miscible window with an ϵ_{pc} range of $1-2\ k_BT$ for α of 0.5, which is a good approximation for short-range H-bonding. From the stability criterion, no phase separation is possible while $\bar{B}_2 > 0$, and indeed in preliminary experiments, stable PEG melts have been produced at volume fractions in excess of 0.3 for all molecular weights studied here.

In order to see a phase transition, PRISM tells us that several key parameters could be manipulated to drive $\bar{B}_2$ negative: ϵ_{pc}, α, D/d, and N. As D/d and N are increased, the miscibility window may narrow. The PMF scales with D/d. As D/d increases, the form of the PMF does not change, but the amplitude of the oscillations grows.[25] If the particles are weakly attractive, an increase in D/d will magnify the attraction, causing $\bar{B}_2$ to get smaller and eventually go negative.[35] On the other hand, if the particles are weakly repulsive, an increase in D/d may stabilize the particles. The narrowing of the window with N is associated with longer chains being able to better bridge two particles.[25,35] The larger dependence on D/d rather than N arises from the segmental length scale playing a larger role in determining particle organization. It is possible that the decreasing trend in $\bar{B}_2$ may be showing a narrowing of the miscibility window with increasing N.

The most significant effect to particle stability leading to a phase transition is likely to be a change in the polymer segment−particle interaction. If the surface interaction is weakened, we would expect negative second viral coefficients and depletion aggregation. If the surface interaction is strengthened, Hooper and Schweizer predict negative second virial coefficients leading to bridging. As previously mentioned, the adsorption of PEG from solution onto silica surfaces is exceptionally strong and is credited to hydrogen bonding between ether oxygens and surface silanol groups. As a result, it is unlikely that we can improve the adsorption strength by increasing the density of surface hydroxyl groups beyond that of the bare silica surface. The ability to hydrogen bond can be lessened by applying a surface coating that reduces the surfaces ability to hydrogen bond. This would lower ϵ_{pc} and likely shift the dispersion to depletion aggregation. We leave exploration of these ideas for future work.

As a second explanation of particle stability, we want to address the possibility of PEG grafting to the particle surface. It has been shown that grafting of PEG can occur at elevated temperatures (113−234 °C) through condensation of PEG hydroxyl end groups with surface silanol groups.[52,53] This is done by dehydrating the silica surface followed by cooking the silica in PEG. In these studies, ethylene glycol oligomers and low MW PEG graft readily to the silica surface. The grafting density decreases for high MW PEG likely due to the reduction of terminal hydroxyl groups in the PEG melt. If we assume the stability arises from polymer grafting, we might expect to estimate an effective particle excluded volume by assuming the grafted polymer adds $2R_{pg}$ to the core particle diameter. Here R_{pg} is the polymer radius of gyration. Assuming a segment length of $d = 0.7$ nm, the radius of gyration of the PEG molecular weights varies from 0.6 nm for PEG400 to 2.9 nm for PEG8000. Assuming the particles with grafted polymer interact like hard spheres with diameters of $D + 2R_{pg}$, $\bar{B}_2$ values would range from 1.2 to 1.4. On the basis of these estimates, we cannot rule out the possibility that PEG may be grafted to the silica surface at our modest temperature of 70 °C, giving steric stabilization to the particles. The potential effects of grafting are currently being explored.

V. Conclusions

In this study, we evaluate the colloidal stability of silica nanoparticles in PEG melts of increasing MW through measurement of particle second virial coefficients. For all molecular weights ≥400, we find the second virial coefficient divided by an equivalent hard sphere to be greater than or equal to one. This indicates that silica filler particles are thermodynamically stable in a PEG melt up to a MW of 8000. We compare these results to particle stability in EG monomer where we find the particles to be significantly more repulsive than in PEG. This repulsion is linked to the particles carrying a negative charge

due to dissociation of surface silanol groups in EG. Particles appear to have negligible charges in PEG as determined from conductivity measurements.

Future work will explore polymer-mediated particle microstructure in concentrated dispersions with increasing polymer MW. We will be interested in the particle packing behavior as the interparticle spacing decreases and adsorbed polymer layers interact with increased particle loading. Particle interactions will be mediated by adsorbed polymer layers. These polymer layers will experience compression forces and may interpenetrate as particles pack together.

Acknowledgment. We acknowledge the UNI-CAT facility at the Advanced Photon Source (APS), Argonne National Laboratory, where SBUSAXS experiments were performed. The UNI-CAT facility is supported by the U.S. DOE under Award DEFG02-91ER45439 through the Frederick Seitz Materials Research Laboratory at the University of Illinois at Urbana−Champaign, the Oak Ridge National Laboratory (U.S. DOE Contract DE-AC05-00OR22725 with UT-Battelle LLC), the National Institute of Standards and Technology (U.S. Department of Commerce), and UOP LLC. The APS is supported by the U.S. DOE, Basic Energy Sciences, Office of Science, under Contract W-31-109-ENG-38. We also acknowledge the Center for Microanalysis of Materials at the University of Illinois, which is partially supported by the U.S. Department of Energy under Grant DEFG02-91-ER45439, where TEM imaging of particles was performed. We appreciate our collaborative relationship and helpful discussions with Ken Schweizer, Justin Hooper, and Lisa Hall. This work was supported by the Nanoscale Science and Engineering Initiative of the National Science Foundation under NSF Award DMR-0117792.

References and Notes

(1) Berriot, J.; Montes, H.; Martin, F.; Mauger, M.; Pyckhout-Hintzen, W.; Meier, G.; Frielinghaus, H. *Polymer* **2003**, *44*, 4909−4919.

(2) Degroot, J. V.; Macosko, C. W.; Kume, T.; Hashimoto, T. *J. Colloid Interface Sci.* **1994**, *166*, 404−413.

(3) Geissler, E.; Hecht, A.-M.; Rochas, C.; Bley, F.; Livet, F.; Sutton, M. *Phys. Rev. E* **2000**, *62*, 8308.

(4) Oberdisse, J.; Deme, B. *Macromolecules* **2002**, *35*, 4397−4405.

(5) Oberdisse, J.; Rharbi, Y.; Boue, F. *Comput. Theor. Polym. Sci.* **2000**, *10*, 207−217.

(6) Ilavsky, J.; Allen, A. J.; Long, G. G.; Jemian, P. R. *Rev. Sci. Instrum.* **2002**, *73*, 1660−1662.

(7) Cohen, Stuart, M. A.; Cosgrove, T.; Vincent, B. *Adv. Colloid Interface Sci.* **1986**, *24*, 143−239.

(8) Cabane, B.; Duplessix, R. *Colloids Surf.* **1985**, *13*, 19−33.

(9) Cabane, B.; Wong, K.; Lindner, P.; Lafuma, F. *J. Rheol.* **1997**, *41*, 531−547.

(10) Cowell, C.; Vincent, B. *J. Colloid Interface Sci.* **1983**, *95*, 573−582.

(11) Daly, S. M.; Przybycien, T. M.; Tilton, R. D. *Biotechnol. Bioeng.* **2005**, *90*, 856−868.

(12) Killmann, E.; Maier, H.; Baker, J. A. *Colloids Surf.* **1988**, *31*, 51−71.

(13) Killmann, E.; Maier, H.; Kaniut, P.; Gutling, N. *Colloids Surf.* **1985**, *15*, 261−276.

(14) Lafuma, F.; Wong, K.; Cabane, B. *J. Colloid Interface Sci.* **1991**, *143*, 9−21.

(15) Liu, S. F.; Lafuma, F.; Audebert, R. *Colloid Polym. Sci.* **1994**, *272*, 196−203.

(16) Liu, S. F.; Legrand, V.; Gourmand, M.; Lafuma, F.; Audebert, R. *Colloids Surf., A* **1996**, *111*, 139−145.

(17) Neel, O.; Ducouret, G.; Lafuma, F. *J. Colloid Interface Sci.* **2000**, *230*, 244−253.

(18) Wong, K.; Lixon, P.; Lafuma, F.; Lindner, P.; Charriol, O. A.; Cabane, B. *J. Colloid Interface Sci.* **1992**, *153*, 55−72.

(19) Tleugabulova, D.; Duft, A. M.; Brook, M. A.; Brennan, J. D. *Langmuir* **2004**, *20*, 101−108.

(20) Vanderbeek, G. P.; Stuart, M. A. C.; Fleer, G. J.; Hofman, J. E. *Macromolecules* **1991**, *24*, 6600−6611.

(21) Cosgrove, T.; Griffiths, P. C.; Lloyd, P. M. *Langmuir* **1995**, *11*, 1457−1463.

(22) Huang, Y. D.; Santore, M. M. *Langmuir* **2002**, *18*, 2158−2165.

(23) Kelly, M. S.; Santore, M. M. *Colloids Surf., A* **1995**, *96*, 199−215.

(24) Ouali, L.; Francois, J.; Pefferkorn, E. *J. Colloid Interface Sci.* **1999**, *215*, 36−42.

(25) Hooper, J. B.; Schweizer, K. S. *Macromolecules* **2005**, *38*, 8858−8869.

(26) Kaplan, P. D.; Rouke, J. L.; Yodh, A. G.; Pine, D. J. *Phys. Rev. Lett.* **1994**, *72*, 582−585.

(27) Dijkstra, M.; van Roij, R.; Evans, R. *Phys. Rev. E* **1999**, *59*, 5744−5771.

(28) Asakura, S.; Oosawa, F. *J. Polym. Sci.* **1958**, *33*, 183−192.

(29) de Hek, H.; Vrij, A. *J. Colloid Interface Sci.* **1982**, *88*, 258−273.

(30) Fuch, M.; Schweizer, K. S. *Europhys. Lett.* **2000**, *51*, 621−627.

(31) Ramakrishnan, S.; Fuchs, M.; Schweizer, K. S.; Zukoski, C. F. *J. Chem. Phys.* **2002**, *116*, 2201−2212.

(32) Shah, S. A.; Chen, Y. L.; Ramakrishnan, S.; Schweizer, K. S.; Zukoski, C. F. *J. Phys.: Condensed Matter* **2003**, *15*, 4751−4778.

(33) Hooper, J. B.; Schweizer, K. S.; Desai, T. G.; Koshy, R.; Keblinski, P. *J. Chem. Phys.* **2004**, *121*, 6986−6997.

(34) Napper, D. H. *Polymeric Stabilization of Colloidal Dispersions*; Academic Press: London, 1983.

(35) Hooper, J. B.; Schweizer, K. S. *Macromolecules* **2006**, *39*, 5133−5142.

(36) Stöber, W.; Fink, A.; Bohn, E. *J. Colloid Interface Sci.* **1968**, *26*, 62−69.

(37) Ho, D. L.; Hammouda, B.; Kline, S. R.; Chen, W. R. *J. Polym. Sci., Part B: Polym. Phys.* **2006**, *44*, 557−564.

(38) Russel, W. B.; Saville, D. A.; Schowalter, W. R. *Colloidal Dispersions*; Cambridge University Press: Cambridge, UK, 1989.

(39) Zimm, B. H. *J. Chem. Phys.* **1948**, *16*, 1093−1099.

(40) Moonen, J.; Pathmamanoharan, C.; Vrij, A. *J. Colloid Interface Sci.* **1989**, *131*, 349−365.

(41) Apfel, U.; Hoerner, K. D.; Ballauff, M. *Langmuir* **1995**, *11*, 3401−3407.

(42) Horner, K. D.; Topper, M.; Ballauff, M. *Langmuir* **1997**, *13*, 551−558.

(43) Ramakrishnan, S.; Fuchs, M.; Schweizer, K. S.; Zukoski, C. F. *Langmuir* **2002**, *18*, 1082−1090.

(44) Weiss, A.; Pötschke, D.; Ballauff, M. *Acta Polym.* **1996**, *47*, 333−339.

(45) Hiemenz, P. C.; Rajagopalan, R. *Principles of Colloid and Surface Chemistry*; Marcel Dekker: New York, 1997.

(46) Kerker, M. *The Scattering of Light*; Academic Press: New York, 1969.

(47) Hermans, J. J. *Recl. Trav. Chim.* **1949**, *68*, 859.

(48) George, A.; Wilson, W. W. *Acta Crystallogr., Sect. D* **1994**, *50*, 361−365.

(49) Kulkarni, A. M.; Chatterjee, A. P.; Schweizer, K. S.; Zukoski, C. F. *Phys. Rev. Lett.* **1999**, *83*, 4554.

(50) Rosenbaum, D.; Zamora, P. C.; Zukoski, C. F. *Phys. Rev. Lett.* **1996**, *76*, 150−153.

(51) Rosenbaum, D. F.; Zukoski, C. F. *J. Cryst. Growth* **1996**, *169*, 752−758.

(52) Balard, H.; Papirer, E.; Rahmani, Y.; Legrand, A. P.; Hommel, H. *Bull. Soc. Chim. Fr.* **1985**, 1139−1142.

(53) Hommel, H.; Legrand, A. P.; Tougne, P.; Balard, H.; Papirer, E. *Macromolecules* **1984**, *17*, 1578−1581.

MA0624346